

Valley Hall Effect and Nonlocal Transport in Strained Graphene

Xian-Peng Zhang,¹ Chunli Huang,^{1,2} and Miguel A. Cazalilla^{3,4}

¹*Department of Physics, National Tsing Hua University, Hsinchu 30013, Taiwan*

²*Division of Physics and Applied Physics, School of Physical and Mathematical Sciences, Nanyang Technological University, Singapore 637371, Singapore*

³*Department of Physics, National Tsing Hua University and National Center for Theoretical Sciences (NCTS), Hsinchu 30013, Taiwan*

⁴*Donostia International Physics Center (DIPC), Manuel de Lardizabal, 4. 20018, San Sebastian, Spain*

Graphene subject to high levels of shear strain leads to strong pseudo-magnetic fields resulting in the emergence of Landau levels. Here we show that, with modest levels of strain, graphene can also sustain a classical valley hall effect (VHE) that can be detected in nonlocal transport measurements. We provide a theory of the strain-induced VHE starting from the quantum Boltzmann equation. This allows us to show that, averaging over short-range impurity configurations destroys quantum coherence between valleys, leaving the elastic scattering time and inter-valley scattering rate as the only parameters characterizing the transport theory. Using the theory, we compute the nonlocal resistance of a Hall bar device in the diffusive regime. Our theory is also relevant for the study of moderate strain effects in the (nonlocal) transport properties of other two-dimensional materials and van der Waals heterostructures.

I. INTRODUCTION

The manipulation of the valley degree of freedom, i.e. the field of *valleytronics*, is currently under intensive research, not only concerning graphene¹⁻⁵ but also other two dimensional (2D) materials.⁶⁻⁹ Indeed, the generation of valley currents has been recently demonstrated² in graphene devices deposited on a Boron Nitride (hBN) substrate. The effect of the hBN substrate is to break the symmetry between the two sublattices of the honeycomb lattice, which opens an energy gap at the (Dirac) point where the conduction and valence bands meet.^{10,11} As a result, a finite Berry curvature, with opposite sign at opposite valleys, endows electrons with an anomalous velocity and leads to a valley-polarized current in the bulk transverse to the applied electric field.^{6,12} This phenomenon, known as the valley Hall effect (VHE), can be detected as large enhancement of the nonlocal resistance in a Hall bar device.^{2,5,27}

Here, we report on a different approach to generate valley-polarized currents in graphene. Since strain can be controlled more easily than the magnitude of the hBN-induced gap, it will allow for a larger tunability of the effect, thus providing a novel link between valleytronics and *straintronics*.^{3,4,13-16} Furthermore, strain also provides a “dual counterpart” to the VHE emerging from Berry curvature in momentum space.^{2,6} This is because in graphene and other 2D materials^{17,18} strain can be described as a (pseudo) gauge field, which induces a (Aharonov-Bohm-like) phase in real space.

A direct consequence of the strain-induced gauge fields is emergence of pseudo-Landau levels, whose experimental observation has been reported in both real¹⁹⁻²¹ and artificial graphene systems.^{22,23} Nevertheless, the observation of quantized valley edge currents (i.e. the quantum VHE), which was predicted in Ref. 13, has not yet been reported. Indeed, the requirements for the latter

are rather stringent, involving devices under relatively high shear strain, low temperatures, and high mobility graphene which is free of atomic-size defects and armchair-like⁴ edges. On the other hand, bulk valley Hall currents can be generated in graphene nanoresonators by the application of pulsed strain, as predicted in Ref. 1. However, the valley currents that are discussed below do not require either pulsed strain or highly strained, high-mobility devices. The strain-induced VHE that we predict should be observable with fairly modest strain levels in hall bar devices. Furthermore, unlike recent work along similar lines,^{1,3,4,24,25} which focuses on nanometer-size devices and ballistic transport, our results apply to much larger and disordered devices in the micrometer scale, where conduction takes places in the diffusive regime. The latter are also potentially much more interesting from the application point of view.

The hallmark of the strain-induced VHE is the emergence of a large nonlocal resistance in Hall bar devices.^{2,5} The nonlocal resistance can be computed from the diffusion equations for the valley polarization. Extending previous treatments of the VHE,^{2,5,27} which have relied on a phenomenological treatment of the diffusion equations, here we provide a microscopic derivation of the diffusion equations starting from the linearized quantum Boltzmann equation derived in Ref. 26. The latter allows us to account for the full quantum coherence of the valley (pseudo-spin) degree of freedom. We are thus able to show that, upon averaging over all the possible equilibrium impurity configurations, the diffusion equations depend on only two scattering rates: the inverse of the mean scattering time and the inter-valley scattering rate. For the latter, we provide expressions that can be used to extract the scattering rates from first principle calculations of a single impurity potential.

Finally, it is worth mentioning that the strain-induced valley Hall currents predicted here are neutral currents

that do not couple to external magnetic fields. Therefore, unlike spin currents,^{27,28} valley currents will not display Hanle precession (i.e. modulation of the nonlocal resistance as a function of the strength of the in-plane magnetic field). Thus, our findings are relevant for the interpretation of some of the nonlocal transport measurements in graphene decorated with hydrogen²⁹ and gold adatoms³⁰, for which Hanle precession was not observed. Indeed, there is no experimental evidence that the devices studied in Refs. 29 and 30 are not subjected to nonuniform strain.³¹ However, the application of the present theory to such experiments, as well as the study of the interplay with other neutral currents, is beyond the scope of this work and will be explored elsewhere.³²

The rest of the article is organized as follows. In the following section, we describe the details of the model as well as its validity regime. In Sec. III, we compute the linear response of a strained graphene and, in particular, the doping and temperature dependence of the valley Hall conductivity. The derivation of the diffusion equation for the valley polarization is provided in Sec. IV. In Sec. V, we compute the nonlocal resistance of a Hall bar device, which provides a convenient way to detect the VHE. In Sec. VI we provide a short summary of our results. Finally, some detailed mathematical expressions are relegated to the Appendix.

II. MODEL

Semiclassically, the electron motion in non-uniformly strained graphene is described using the following set of equations:

$$\dot{\mathbf{r}} = \mathbf{u}_k, \quad \dot{\mathbf{k}} = (e\mathbf{E} + \tau_z \dot{\mathbf{r}} \times \mathcal{B}_s), \quad (1)$$

where \mathbf{r} and \mathbf{k} are the average position and momentum of a narrow wave packet of Bloch states, $\epsilon_k = \lambda v_F |\mathbf{k}|$ the electron dispersion ($\lambda = +1$ for the conduction and $\lambda = -1$ for the valence band, respectively), and $\mathbf{u}_k = \nabla_{\mathbf{k}} \epsilon_k = \lambda v_F \mathbf{k} / |\mathbf{k}|$ the carrier group velocity (henceforth we set $\hbar = 1$). In addition, \mathbf{E} is the applied electric field, $e < 0$ the electron charge, and $\tau_z \mathcal{B}_s$ is strain-induced pseudo-magnetic field.^{11,13–15} Note that, because strain does not break time-reversal invariance (unlike a real magnetic field), the sign of the magnetic field is opposite at opposite valleys. In terms of the strain tensor^{11,14,15} $u_{\alpha\beta}$, $\mathcal{B}_s = \nabla \times \mathcal{A}_s$ where $\mathcal{A}_s = \frac{\beta}{a} (u_{xx} - u_{yy}, -2u_{xy})$ is the pseudo gauge field. Here $a = 1.42 \text{ \AA}$ is the carbon-carbon distance and¹³ $\beta \simeq 2$. In the absence of an electric field (i.e. $\mathbf{E} = 0$), Eq. (1) predicts that a wave packet of mean momentum $\mathbf{k}_0 \neq 0$ moves in a circular orbit and in opposite directions depending on whether \mathbf{k}_0 lies closer to the K or K' valley. Such a valley-dependent circular motion of electron wavepackets has been observed numerically.³³

When quantized, the circular orbits lead to pseudo-Landau levels^{11,13,16} (pLLs) with energy dispersion $\epsilon_n =$

$\pm \Omega_c \sqrt{n}$, where $\Omega_c = \sqrt{2v_F^2 |\mathcal{B}_s|}$ is the cyclotron frequency of graphene. In this work, however, we will explore the semiclassical regime, for which pLL are absent due to the broadening induced by disorder and/or temperature (T). This is the case when the distance between consecutive Landau levels, i.e. $\Delta_n = \epsilon_{n+1} - \epsilon_n$, is smaller or comparable to $\min\{k_B T, \tau_D^{-1}\}$, where τ_D^{-1} is the impurity scattering rate (see below). For large pLL filling factor, i.e. for $\mu \gg \Omega_c$, where $\mu = v_F k_F$ is the Fermi energy (at $T = 0$) and k_F the Fermi momentum, $\Delta_n \simeq \Omega_c n^{-1/2}$. Taking into account that $\sqrt{n} \simeq \mu / \Omega_c$, the condition $\Delta_n \tau_D \lesssim 1$ translates into $\omega_c \tau_D \lesssim 1$, where $\omega_c = \Omega_c^2 / \mu = v_F |e \mathcal{B}_s| / k_F$. Below, we shall see that the modified cyclotron frequency ω_c naturally emerges when the Boltzmann kinetic equation is applied to describe doped graphene. Besides the low pseudo-magnetic field (i.e low strain) limit, our results are also applicable in high field limit where $\omega_c \tau_D \gg 1$ provided the temperature $T \gg \omega_c / k_B$ (where k_B is Boltzmann's constant).

Under the conditions stated above, we can use the following linearized Boltzmann equation (BE) to describe doped strained graphene:

$$\partial_t \delta n_k + \dot{\mathbf{r}} \cdot \nabla_r \delta n_k + \dot{\mathbf{k}} \cdot \nabla_k [n_k^0 + \delta n_k] = \mathcal{I}[\delta n_k], \quad (2)$$

where δn_k is deviation of the electron distribution from the equilibrium distribution, i.e. $\delta n_k = n_k - n_k^0$, where $n_k^0 = n^0(\epsilon_k - \mu)$, being $n^0(\epsilon) = [e^{\epsilon/k_B T} + 1]^{-1}$ the Fermi-Dirac distribution at temperature T and chemical potential μ . Note that, in order to correctly account for the quantum entanglement between the two valleys within the $\mathbf{k} \cdot \mathbf{p}$ theory,¹¹ $\delta n_{\mathbf{k}}$ must be treated as a 2×2 density matrix acting on the space of valley pseudo-spinors.

In Eq. (2), the collision integral $\mathcal{I}[\delta n_{\mathbf{k}}]$ describes the effect of disorder. Its form has been derived in Ref. 26, extending the work of Kohn and Luttinger³⁴ in order to account for the effects of disorder on the electron internal degrees of freedom, such as the valley pseudo-spin. To leading order in the impurity density, n_{imp} ,

$$\mathcal{I}[\delta n_{\mathbf{k}}] = 2\pi n_{\text{imp}} \sum_{\mathbf{p}} \delta(\epsilon_k - \epsilon_p) \left[T_{kp}^+ \delta n_p T_{pk}^- - \frac{1}{2} \left\{ \delta n_k T_{kp}^+ T_{pk}^- + T_{kp}^+ T_{pk}^- \delta n_k \right\} \right], \quad (3)$$

where T_{kp}^{\pm} is the scattering matrix for a single impurity (the system area is assumed to be unity).

At low temperatures, the dominant mechanism that limits the diffusion of bulk valley currents is the inter-valley scattering caused by atomic-size impurities and defects. Here we consider a random ensemble of atomic-size impurities, which are assumed to reside on the honeycomb lattice sites (e.g. vacancies). Our considerations can be generalized to the other types of impurity potentials classified on symmetry grounds in Ref. 35. The effect of random strain fluctuations, which dominate transport in high-quality devices on substrates like hBN, has been studied elsewhere,³⁶ and will be neglected here.

Within the $\mathbf{k} \cdot \mathbf{p}$ theory, the potential for one such impurity takes the following form:^{35,37,38}

$$V(\mathbf{r}) = [v_0\mathbb{1} + sv_z\sigma_z] \delta(\mathbf{r}) + v_{xy}(\mathbb{1} + s\sigma_z)(u_x\tau_x + iu_y\sigma_z\tau_y) \delta(\mathbf{r}), \quad (4)$$

where the Pauli matrices σ_α and τ_α ($\alpha = x, y, z$) describe the sublattice and valley pseudo-spin, respectively. In the above expression, the terms in the first line ($\propto v_0, v_z$) conserve the valley pseudo-spin τ_z while the terms in the second line induce inter-valley scattering. The Ising variable $s = +1$ ($s = -1$) when the impurity sits on the A (B) sublattice. The vector $\mathbf{u} = (u_x, u_y) \in S = \{(1, 0), (-\frac{1}{2}, \frac{\sqrt{3}}{2}), (-\frac{1}{2}, -\frac{\sqrt{3}}{2})\}$ parametrizes the inter-valley scattering potential.^{35,37,38} The impurities are assumed to form a completely disordered ensemble, which is the most stable configuration at high doping and temperatures of interest here.^{35,38} Thus, the configurational variables ($s_l = \pm 1, \mathbf{u}_l \in S$) can take all the six possible values allowed by symmetry with equal probability. Hence, upon solving the scattering problem, the band-projected (on shell) T-matrix can be obtained, and it takes the general form, $T_{kp}^+ = A_{kp}\mathbb{1} + \mathbf{B}_{kp} \cdot \boldsymbol{\tau}$, where $\mathbf{B}_{kp} = \mathbf{B}_{kp}^\parallel + \hat{\mathbf{z}} B_{kp}^\perp$, describes the valley-dependent scattering with $\hat{\mathbf{z}} \cdot \mathbf{B}_{kp}^\parallel = 0$, and

$$A_{kp} = \gamma_0(k) \cos \frac{\theta}{2}, \quad (5)$$

$$B_{kp}^\perp = is\tau_z\gamma_z(k) \sin \frac{\theta}{2}, \quad (6)$$

$$\mathbf{B}_{kp}^\parallel = \lambda\gamma_{xy}(k) \left[s \left(u_x \cos \frac{\phi}{2} + u_y \sin \frac{\phi}{2} \right) \hat{\mathbf{x}} + \left(-u_x \sin \frac{\phi}{2} + u_y \cos \frac{\phi}{2} \right) \hat{\mathbf{y}} \right], \quad (7)$$

where $\theta = \varphi_k - \varphi_p$ and $\phi = \varphi_k + \varphi_p$, and $\varphi_k = \tan^{-1}(k_y/k_x)$. The functions $\gamma_0(k)$, $\gamma_z(k)$ and $\gamma_{xy}(k)$ depend on $k = |\mathbf{k}|$ (where \mathbf{k} is the momentum of the incoming electron) and the potential parameters v_0, v_z, v_{xy} (see e.g. Refs. 37 and 39 for details of such scattering calculations). However, the important point to notice is that while B_{kp}^\perp depends linearly on the Ising variable s , $\mathbf{B}_{kp}^\parallel$ depends both on s and u_x, u_y , in a way such that $\overline{B_{kp}^\perp \mathbf{B}_{kp}^\parallel} = \mathbf{0}$, where $\overline{}$ stands for average over the impurity configurations.

III. LINEAR RESPONSE

In order to obtain the response of the system, we parametrize $\delta n_k = \rho_k\mathbb{1} + \mathcal{P}_k \cdot \boldsymbol{\tau}$, where ρ_k describes the charge fluctuations and $\mathcal{P}_k = \mathcal{P}_k^\parallel + \hat{\mathbf{z}} \mathcal{P}_k^\perp$ (with $\hat{\mathbf{z}} \cdot \mathcal{P}_k^\parallel = 0$) the valley pseudo-spin fluctuations of the electron distribution, δn_k . Summing over the impurity configurations, the kinetic equations for ρ_k, \mathcal{P}_v on one side, and

\mathcal{P}_v^\perp , on the other side, decouple. Thus, in what follows, we focus on the equations for ρ_k, \mathcal{P}_v , which describe the valley Hall effect of interest here. In addition, the collision integral for the latter is found to be parametrized by two scattering rates: the Drude scattering rate $\tau_D^{-1} = \frac{n_{\text{imp}}k}{4v_F}(|\gamma_0|^2 + 3|\gamma_z|^2 + 4|\gamma_{xy}|^2)$, and the inter-valley scattering rate $\tau_v = \frac{n_{\text{imp}}k}{4v_F}(8|\gamma_{xy}|^2)$.

In the steady state, we employ the ansatz²⁶ $\rho_k = (\delta\mu + \mathbf{u}_c \cdot \mathbf{k}) [-\partial_\mu n_k^0]$ and $\mathcal{P}_k = [h_v \hat{\mathbf{n}}_0 + \hat{\mathbf{n}}_1 (\mathbf{u}_v \cdot \mathbf{k})] [-\partial_\mu n_k^0]$, which allows us to obtain the constitutive relations by multiplying Eq. (2) by $\mathbf{u}_k(\mathbb{1}, \tau_z)$, tracing over \mathbf{k}, λ and valley pseudo-spin. Thus,

$$\mathbf{J} = -\mathcal{D} \nabla_r \delta n(\mathbf{r}) + \omega_c \tau_D (\hat{\mathbf{z}} \times \mathcal{J}) + \sigma_D \mathbf{E}(\mathbf{r}), \quad (8)$$

$$\mathcal{J} = -\mathcal{D} \nabla_r \mathcal{P}(\mathbf{r}) + \omega_c \tau_D (\hat{\mathbf{z}} \times \mathcal{J}), \quad (9)$$

where $\delta n = g_s e \text{Tr} \sum_k \delta n_k$ and $\mathbf{J} = eg_s \text{Tr} \sum_k [\mathbf{u}_k \delta n_k]$ are the particle density and charge current, respectively. $\mathcal{P} = g_s e \text{Tr} \sum_k [\tau_z \delta n_k]$ and $\mathcal{J} = eg_s \text{Tr} [\mathbf{u}_k \tau_z \delta n_k]$ are the valley polarization and current, respectively (g_s is the spin degeneracy). In the above expression $\sigma_D = ne^2 \tau_D / (m_F)$ ($m_F = k_F / v_F$ and n is the carrier density) is the Drude conductivity and $\mathcal{D} = v_F^2 \tau_D / 2$ the diffusion coefficient. The last equation describes the classical VHE, while the second term on the right-hand side of Eq. (8) describes the inverse VHE. Next, we solve Eq. (8) and (9) for the charge \mathbf{J} and valley current \mathcal{J} , which yields

$$\mathbf{J} = -\mathcal{D}_\parallel \nabla_r \delta n(\mathbf{r}) + \mathcal{D}_\perp \hat{\mathbf{z}} \times \nabla_r \mathcal{P}(\mathbf{r}) + \sigma_\parallel \mathbf{E}(\mathbf{r}), \quad (10)$$

$$\mathcal{J} = -\mathcal{D}_\parallel \nabla_r \mathcal{P}(\mathbf{r}) + \mathcal{D}_\perp \hat{\mathbf{z}} \times \nabla_r \delta n(\mathbf{r}) + \sigma_\perp \hat{\mathbf{z}} \times \mathbf{E}(\mathbf{r}), \quad (11)$$

where the longitudinal (transverse) diffusion constant \mathcal{D}_\parallel (\mathcal{D}_\perp) and longitudinal (transverse) conductivity σ_\parallel (σ_\perp) are given by the following expressions:

$$\mathcal{D}_\parallel = \frac{\mathcal{D}}{1 + \omega_c^2 \tau_D^2}, \quad \mathcal{D}_\perp = \frac{\omega_c \tau_D \mathcal{D}}{1 + \omega_c^2 \tau_D^2}, \quad (12)$$

$$\sigma_\parallel = \frac{\sigma_D}{1 + \omega_c^2 \tau_D^2}, \quad \sigma_\perp = \frac{\omega_c \tau_D \sigma_D}{1 + \omega_c^2 \tau_D^2}. \quad (13)$$

Note that, for a uniform electric field, both $\nabla_r \delta n(\mathbf{r})$ and $\nabla_r \mathcal{P}(\mathbf{r})$ vanish, and we obtain the linear response of the system, $\mathbf{J} = \sigma_\parallel \mathbf{E}$ and $\mathcal{J} = \sigma_\perp (\hat{\mathbf{z}} \times \mathbf{E})$. The longitudinal charge conductivity σ_\parallel is reduced by the strain pseudo-magnetic field in a way similar to a real magnetic field. Similar to the conventional Hall effect, both the inverse and direct VHE can be characterized by a figure of merit, namely the *valley Hall angle* θ , which is defined as follows (see Appendix for the definitions of $\sigma_\perp(T), \sigma_\parallel(T)$):

$$\tan \theta(T) = \frac{\sigma_\perp(T)}{\sigma_\parallel(T)}, \quad (14)$$

At zero temperature, $\tan \theta(T=0) = \omega_c \tau_D$. The dependence of $\theta(T)$ on the chemical potential μ at different

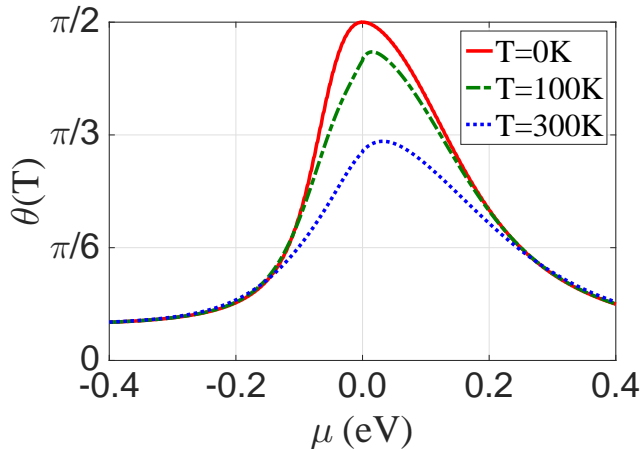


FIG. 1. (color online) The valley Hall angle, $\theta(T)$ is plotted against chemical potential μ for different temperatures $T = 0, 100, 300\text{K}$. The parameters used are: $\mathcal{B}_s = 0.3\text{ T}$, $n_{\text{imp}} = 5.0 \times 10^{11}\text{ cm}^{-2}$, the impurity (vacancy) potential (cf. Eq. 4) is parametrized by $v_0 = 100\text{ eV}$, $v_z = v_{xy} = 3\text{ eV}$, impurity radius $R = 0.142\text{ nm}$, and cut-off momentum $k_c = 1 \times 10^{-9}\text{ m}^{-1}$.

temperatures is shown in Fig. 1. We find that the valley Hall angle can approach $\frac{\pi}{2}$ at low doping and low temperatures. This is because the pseudo cyclotron frequency ω_c is inversely proportional to μ and τ_D is resonantly enhanced in the neighborhood of the Dirac point. However, the semiclassical theory becomes less reliable close to the Dirac point where $\mu = 0$. Indeed, $\theta \frac{\pi}{2}$ at low doping and $T = 0$, which implies that $\omega_c \tau_D \gg 1$, meaning that the semiclassical theory ceases to be valid, as discussed above. Fortunately, as temperature T is increased, thermal fluctuations suppress the magnitude of $\theta(T)$ at small μ and we find that a semiclassical regime where $\omega_c \tau_D \gtrsim \theta(T) \gtrsim 1$ also exists at high temperature and low doping.

IV. DIFFUSION OF THE VALLEY POLARIZATION

The above quantum Boltzmann equation also allows us to obtain the continuity equations for the charge and the valley current. After multiplying Eq. (2) by $(\mathbb{1}, \tau_z)$ and taking the trace after summing over λ and \mathbf{k} , we obtain (in the steady state) $\nabla \cdot \mathbf{J} = 0$, for the charge current and $\nabla_r \cdot \mathcal{J} + \mathcal{P}/\tau_v = 0$, for the valley current. By combining the last equation with Eq. (11), the diffusion equation for the valley polarization is obtained:

$$\mathcal{D}_{\parallel} \nabla_r^2 \mathcal{P}(\mathbf{r}) - \frac{\mathcal{P}(\mathbf{r})}{\tau_v} = S(\mathbf{r}), \quad (15)$$

where $S(\mathbf{r}) = \hat{z} \cdot \nabla_r \times [\sigma_{\perp}(\mathbf{r}) \mathbf{E}(\mathbf{r})]$ is the source of the diffusion. For uniform pseudo-magnetic field, the source term vanishes everywhere except at the device boundary

where the strain-induced pseudo-magnetic field vanishes. Eq. (15) indicates the existence of the following length scale that controls the diffusion of valley polarization:

$$\ell_v = \sqrt{\mathcal{D}_{\parallel} \tau_v} = L_v (1 + \omega_c^2 \tau_D^2)^{-1/2}, \quad (16)$$

where $L_v = \sqrt{\mathcal{D}_{\parallel} \tau_v}$. In Fig. 2(a), we have plotted the length scale ℓ_v against the chemical potential for different values of strength of the pseudo-magnetic field. We find that the magnitude of ℓ_v decreases with the magnitude of the pseudo-magnetic field, as expected from Eq. (16). For the present choice of parameters, note that the resulting valley diffusion length ℓ_v (i.e. about $6\text{ }\mu\text{m}$ at $\mu = 0.1\text{ eV}$) is, in most regimes, larger than the width of the device, $W = 0.5\text{ }\mu\text{m}$. However, as shown in the next section, the decay of the nonlocal resistance along the channel direction is controlled by L_v rather than ℓ_v .

V. NONLOCAL RESISTANCE

Following Beocchini *et al.*,⁵ we solve the diffusion equation for a Hall bar device geometry, consisting of a channel of width W , which we assume to be infinitely long. Thus, the solution of the diffusion equations can be found by imposing suitable boundary conditions (BCs): i) On the charge current: $J_y(x, y = \pm W/2) = I \delta(x)$. This BC describes the current injection (extraction) along the y direction ii) On the valley current: $\mathcal{J}_y(x, y = \pm W/2) = 0$, implying that no valley current flows across the device boundary.

The solution can be simplified by taking $\delta n(\mathbf{r}) \simeq 0$, which amounts to assuming complete screening of the electric field in the device.⁵ Thus, the electrostatic potential $\phi(\mathbf{r})$ obeys the Laplace equation, $\nabla^2 \phi(\mathbf{r}) = 0$. Using Eq. (10) and (11), the BCs can be recast as:

$$I \delta(x) = [-\mathcal{D}_{\perp} \partial_x \mathcal{P}(\mathbf{r}) - \sigma_{\parallel} \partial_y \phi(\mathbf{r})]_{y=\pm W/2}, \quad (17)$$

$$0 = [-\mathcal{D}_{\parallel} \partial_y \mathcal{P}(\mathbf{r}) - \sigma_{\perp} \partial_x \phi(\mathbf{r})]_{y=\pm W/2}, \quad (18)$$

where we have dropped the terms containing $\delta n(\mathbf{r})$. We see that the BCs couple the Laplace equation for $\phi(\mathbf{r})$ with the diffusion equation for $\mathcal{P}(\mathbf{r})$. Eq. (15) together with the Laplace equation can be solved using Eq. (17) and (18) as BCs. Thus, we obtain:

$$\phi(\mathbf{r}) = -I \rho_c \int_{-\infty}^{+\infty} \frac{dk}{2\pi} \frac{e^{+ikx} \omega(k) \sinh(ky)}{F(k) \sinh\left(\frac{kW}{2}\right)}, \quad (19)$$

$$\mathcal{P}(\mathbf{r}) = \frac{I \tan(\theta)}{i \mathcal{D}_{\parallel}} \int_{-\infty}^{+\infty} \frac{dk}{2\pi} \frac{e^{+ikx} \cosh(\omega(k)y)}{F(k) \sinh\left(\frac{\omega(k)W}{2}\right)}, \quad (20)$$

where $\rho_c = 1/\sigma_{\parallel}$, $F(k) = \tan^2(\theta) k \coth\left(\frac{\omega(k)W}{2}\right) + \omega(k) \coth\left(\frac{kW}{2}\right)$, and $\omega(k) = \sqrt{k^2 + \ell_v^{-2}}$.

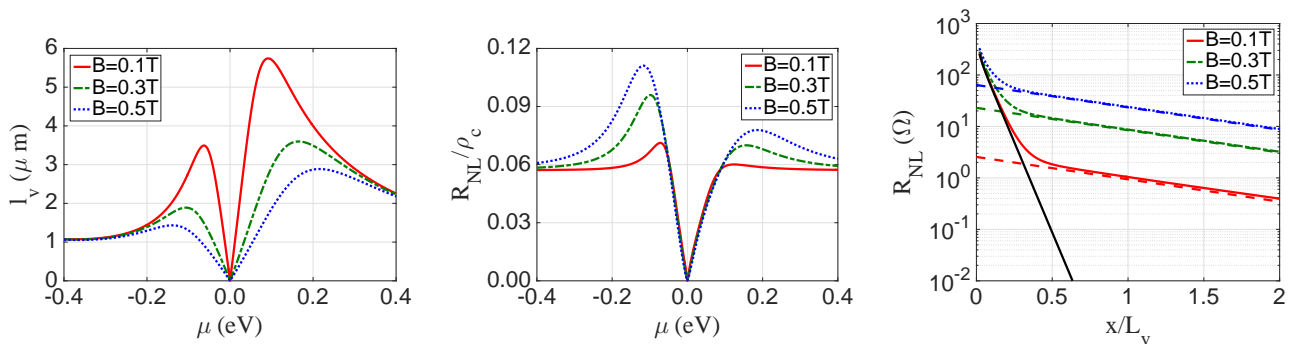


FIG. 2. (color online) (a) ℓ_v , in μm , versus the chemical potential μ . (b) Nonlocal resistance R_{NL} (in units of ρ_c) evaluated at $x = 1 \mu\text{m}$ as a function of chemical potential μ . (c) Nonlocal resistance R_{NL} (in logarithmic scale) as a function of chemical potential x/L_v for fixed chemical potential $\mu = 0.15 \text{ eV}$ ($L_v \simeq 5 \mu\text{m}$). Note that the decay is controlled by the same length scale L_v for all values of the pseudo-magnetic field. The latter is induced by applying along the y direction an average (uniaxial) strain of 0.4%, 1.2% and 2.0%, respectively, to a ribbon of width $W = 1 \mu\text{m}$. The parameters are the same as for Fig. 1.

Hence, the nonlocal resistance can be obtained from $R_{\text{NL}}(x) = [\phi(x, -W/2) - \phi(x, W/2)]/I$. Substituting Eq. (19) yields:⁵

$$R_{\text{NL}}(x) = 2\rho_c \int_{-\infty}^{+\infty} \frac{dk}{2\pi k} e^{+ikx} \frac{\omega(k)}{F(k)}. \quad (21)$$

For $\theta = 0$, the nonlocal resistance reduces to the ohmic contribution:

$$R_{\text{NL}}^0(x) = \frac{2\rho_c}{\pi} \ln \left| \coth \left(\frac{\pi x}{2W} \right) \right|. \quad (22)$$

Fig. 2 shows the results of numerically integrating Eq. (21). At a fixed distance $x = 1 \mu\text{m}$ away from the current injection point, Fig. 2(b) shows the nonlocal resistance R_{NL} against the chemical potential μ , for different values of the pseudo-magnetic field, B_s . The nonlocal resistance arising from the combined effect of VHE and inverse VHE is enhanced at low doping. Panel (c) in Fig. 2 shows the dependence of the nonlocal resistance $R_{\text{NL}}(x)$ with x/L_v at fixed chemical potential $\mu = 0.1 \text{ eV}$. Nonuniform strain enhances the nonlocal resistance relative to its ohmic value. At large $|x|$, and for $W \ll \ell_v$, R_{NL} decays according to:

$$R_{\text{NL}}(x) = \rho_c \frac{W}{2L_v} \frac{\tan^2(\theta)}{1 + \tan^2(\theta)} e^{-|x|/L_v}, \quad (23)$$

which agrees well with the numerical results for $|x| \gg \ell_v \gg W$ (cf. Fig. 2, showing that the ohmic contribution, cf. Eq. (22) is also much smaller in this limit). Note that, in this regime, the decay is controlled by L_v rather than the length scale ℓ_v introduced in Eq. (16). This can be understood from the fact that Eq. (21) is obtained by solving the coupled diffusion and Laplace equations, which takes into account the buildup of electrostatic potential (due to the inverse valley Hall effect) along the channel. The latter modifies the decay of $R_{\text{NL}}(x)$ by effectively replacing $\ell_v = L_v(1 + \omega_c^2 \tau_D)^{1/2}$ by $L_v = \sqrt{D\tau_v}$.

VI. SUMMARY AND OUTLOOK

We have developed a theory of the strain-induced classical valley Hall effect (VHE). Specifically, using the quantum Boltzmann equation, we have provided a microscopic derivation of the equations governing the diffusion of valley polarization. The latter have been solved for a Hall bar device geometry with subject to nonuniform strain leading to uniform pseudo-magnetic field. The observable nonlocal resistance of the device has been obtained. We found that for low doping the figure of merit of the VHE, namely the valley Hall angle, $\theta(T)$ can be of order unity even at room temperature. The nonlocal resistance of the device decays exponentially.

Finally, it is interesting to consider the effect of a strain configuration leading to a slowly varying (on the scale of the Fermi wavelength) pseudo-magnetic field. The equations derived here are also applicable in this case, with the caveat that in such a case $\omega_c \tau_D$ becomes space dependent. This complicates the solution of the diffusion equation, Eq. (15), as the source term on the right-hand side $S(\mathbf{r})$ will not be a boundary term. In addition, the diffusion coefficient $D_{\parallel} = D_{\parallel}(\mathbf{r})$ is now a function of the position in the device. However, qualitative, one can still expect a nonlocal signal to exist even if the sing of the pseudo-magnetic field fluctuates in space because the nonlocal resistance depends quadratically on the valley Hall angle $\theta \sim \omega_c \tau_D$ as it arises from the combination of the direct and inverse valley Hall effects.

ACKNOWLEDGMENTS

This work is supported by the Ministry of Science and Technology (Taiwan) under contract number NSC 102-2112-M-007-024-MY5, and Taiwan's National Center of Theoretical Sciences (NCTS). We thank F. Guinea, A. Kaverzin, and J. Song for useful discussion.

Appendix: Temperature dependent conductivities

In this Appendix, we provide the expressions to compute the charge (σ_{\parallel}) and spin Hall (σ_{\perp}) conductivities at temperature $T > 0$:

$$\sigma_{\parallel}(T) = \frac{e^2}{2\pi} \int d\epsilon |\epsilon| \frac{\tau_D [-\partial_{\mu} n^0(\epsilon - \mu)]}{(1 + \omega_c^2 \tau_D^2)}, \quad (\text{A.1})$$

$$\sigma_{\perp}(T) = \frac{e^2}{2\pi} \int d\epsilon |\epsilon| \frac{\omega_c \tau_D^2 [-\partial_{\mu} n^0(\epsilon - \mu)]}{(1 + \omega_c^2 \tau_D^2)}. \quad (\text{A.2})$$

where both τ_D and ω_c are energy (i.e. Fermi momentum) dependent and $n^0(\epsilon) = [e^{\epsilon/k_B T} + 1]^{-1}$ is the Fermi-Dirac distribution. Notice that for $T \rightarrow 0$, we recover Eq. (13).

-
- ¹ Y. Jiang, T. Low, K. Chang, M. I. Katsnelson, and F. Guinea, *Phys. Rev. Lett.* **110**, 046601 (2013).
- ² R. Gorbachev, J. Song, G. Yu, A. Kretinin, F. Withers, Y. Cao, A. Mishchenko, I. Grigorieva, K. Novoselov, L. Levitov, *et al.*, *Science* **346**, 448 (2014).
- ³ D. A. Gradinar, M. Mucha-Kruczyński, H. Schomerus, and V. I. Fal'ko, *Phys. Rev. Lett.* **110**, 266801 (2013).
- ⁴ D. A. Cosma, M. Mucha-Kruczyński, H. Schomerus, and V. I. Fal'ko, *Phys. Rev. B* **90**, 245409 (2014).
- ⁵ M. Beconcini, F. Taddei, and M. Polini, *Phys. Rev. B* **94**, 121408 (2016).
- ⁶ D. Xiao, M.-C. Chang, and Q. Niu, *Reviews of modern physics* **82**, 1959 (2010).
- ⁷ Y. Shimazaki, M. Yamamoto, I. V. Borzenets, *et al.*, *Nature Physics* **11**, 1032 (2015).
- ⁸ E. J. Sie, J. W. McIver, *et al.*, *Nature Materials* **14**, 290 (2015).
- ⁹ J. Lee, K. F. Mak, and J. Shan, *Nature Nanotechnology* (2016).
- ¹⁰ A. H. Castro Neto, F. Guinea, N. Peres, K. S. Novoselov, and A. K. Geim, *Rev. Mod. Phys.* **81**, 109 (2009).
- ¹¹ M. I. Katsnelson, *Graphene: carbon in two dimensions* (Cambridge University Press, 2012).
- ¹² F. D. M. Haldane, *Phys. Rev. Lett.* **93**, 206602 (2004).
- ¹³ F. Guinea, M. Katsnelson, and A. Geim, *Nature Physics* **6**, 30 (2010).
- ¹⁴ M. A. Vozmediano, M. Katsnelson, and F. Guinea, *Physics Reports* **496**, 109 (2010).
- ¹⁵ B. Amorim, A. Cortijo, F. de Juan, A. G. Grushin, F. Guinea, A. Gutiérrez-Rubio, H. Ochoa, V. Parente, R. Roldán, P. San-José, P. Schiefele, M. Sturla, and M. A. H. Vozmediano, *Physics Reports* **617**, 1 (2016).
- ¹⁶ e. a. Mikkel Settnes, Nicolas Leconte, arXiv:1607.07300 (2016).
- ¹⁷ M. A. Cazalilla, H. Ochoa, and F. Guinea, *Phys. Rev. Lett.* **113**, 077201 (2014).
- ¹⁸ A. J. Pearce, E. Mariani, and G. Burkard, *Phys. Rev. B* **94**, 155416 (2016).
- ¹⁹ N. Levy, S. A. Burke, K. L. Meaker, M. Panlasigui, A. Zettl, F. Guinea, A. H. C. Neto, and M. F. Crommie, *Science* **329**, 544 (2010).
- ²⁰ H. Shioya, S. Russo, M. Yamamoto, M. F. Craciun, and S. Tarucha, *Nano Letters* **15**, 7943 (2015).
- ²¹ S.-Y. Li, K.-K. Bai, L.-J. Yin, J.-B. Qiao, W.-X. Wang, and L. He, *Phys. Rev. B* **92**, 245302 (2015).
- ²² K. K. Gomes, W. Mar, W. Ko, F. Guinea, and H. C. Manoharan, *Nature* **483**, 306 (2012).
- ²³ M. C. Rechtsman, J. M. Zeuner, A. Tunnermann, S. Nolte, M. Segev, and A. Szameit, *Nat Photon* **7**, 153 (2013).
- ²⁴ S. P. Milovanovic and F. Peeters, arxiv:1610.09916 (2016).
- ²⁵ R. Carrillo-Bastos, C. León, D. Faria, A. Latgé, E. Y. Andrei, and N. Sandler, *Phys. Rev. B* **94**, 125422 (2016).
- ²⁶ C. Huang, Y. D. Chong, G. Vignale, and M. A. Cazalilla, *Phys. Rev. B* **93**, 165429 (2016).
- ²⁷ D. A. Abanin, A. V. Shytov, L. S. Levitov, and B. I. Halperin, *Phys. Rev. B* **79**, 035304 (2009).
- ²⁸ J. Balakrishnan, G. K. W. Koon, A. Avsar, Y. Ho, J. H. Lee, M. Jaiswal, S.-J. Baeck, J.-H. Ahn, A. Ferreira, M. A. Cazalilla, and A. H. Castro Neto, *Nature Communications* **5**, 4748 (2014).
- ²⁹ A. A. Kaverzin and B. J. van Wees, *Phys. Rev. B* **91**, 165412 (2015).
- ³⁰ Y. Wang, X. Cai, J. Reutt-Robey, *et al.*, *Phys. Rev. B* **92**, 161411 (2015).
- ³¹ A. A. Kaverzin, private communication.
- ³² X.-P. Zhang, C. Huang, and M. A. Cazalilla, to be published.
- ³³ D. R. da Costa, A. Chaves, G. A. Farias, L. Covaci, and F. M. Peeters, *Phys. Rev. B* **86**, 115434 (2012).
- ³⁴ J. M. Luttinger and W. Kohn, *Phys. Rev.* **109**, 1892 (1958).
- ³⁵ V. V. Cheianov, O. Syljuåsen, B. L. Altshuler, and V. Fal'ko, *Phys. Rev. B* **80**, 233409 (2009).
- ³⁶ N. J. G. Couto, D. Costanzo, S. Engels, D.-K. Ki, K. Watanabe, T. Taniguchi, C. Stampfer, F. Guinea, and A. F. Morpurgo, *Phys. Rev. X* **4**, 041019 (2014).
- ³⁷ D. M. Basko, *Physical Review B* **78**, 115432 (2008).
- ³⁸ S. Kopylov, V. Cheianov, B. L. Altshuler, and V. I. Fal'ko, *Phys. Rev. B* **83**, 201401 (2011).
- ³⁹ H.-Y. Yang, C. Huang, H. Ochoa, and M. A. Cazalilla, *Phys. Rev. B* **93**, 085418 (2016).